Nanoscale Research Letters
a SpringerOpen Journal

NANO EXPRESS Open Access

Atomic layer deposition of high-density Pt nanodots on Al_2O_3 film using $(MeCp)Pt(Me)_3$ and O_2 precursors for nonvolatile memory applications

Shi-Jin Ding*, Hong-Bing Chen, Xing-Mei Cui, Sun Chen, Qing-Qing Sun, Peng Zhou, Hong-Liang Lu, David Wei Zhang and Chen Shen

Abstract

Pt nanodots have been grown on Al_2O_3 film via atomic layer deposition (ALD) using $(MeCp)Pt(Me)_3$ and O_2 precursors. Influence of the substrate temperature, pulse time of $(MeCp)Pt(Me)_3$, and deposition cycles on ALD Pt has been studied comprehensively by scanning electron microscopy, transmission electron microscopy, and X-ray photoelectron spectroscopy. Therefore, Pt nanodots with a high density of approximately 2×10^{12} cm^{-2} have been achieved under optimized conditions: 300°C substrate temperature, 1 s pulse time of $(MeCp)Pt(Me)_3$, and 70 deposition cycles. Further, metal-oxide-semiconductor capacitors with Pt nanodots embedded in ALD Al_2O_3 dielectric have been fabricated and characterized electrically, indicating noticeable electron trapping capacity, efficient programmable and erasable characteristics, and good charge retention.

Keywords: Atomic layer deposition, Pt nanodots, Nonvolatile memory

Background

Platinum (Pt) nanodots or nanoparticles have been attracting more and more attention due to their various potential applications. As a catalyst, Pt nanodots have been extensively used in the petroleum reforming and petrochemical industries as well as in fuel cells because of their excellent catalytic activity [1-4]. On the other hand, Pt nanodots have also been investigated for memory devices that utilize discrete metal nanodots as charge storage medium [5,6]. This is attributed to the potential that the nanodot-based memories can lessen the impact of localized oxide defects, lateral coupling of charge storage layers between adjacent devices, and stress-induced leakage current [7]. Moreover, Pt has a high work function of 5.1 eV, low diffusivity, and excellent thermal stability [6-8]. Therefore, the employment of Pt nanodots can obtain a deep potential well in memory devices to ensure good data retention, together with good compatibility with CMOS processing. However, most researchers used high-temperature rapid thermal annealing (RTA) of ultrathin Pt films to achieve high-density Pt nanodots [5,8,9], which might cause the formation of an additional interfacial layer between the high-permittivity (high-*k*) tunnel layer and silicon substrate as well as crystallization of the tunnel layer.

In recent years, atomic layer deposition (ALD) of Pt nanoparticles have been investigated on various surfaces such as micron-sized porous silica gel particles [10], $SrTiO_3$ nanocubes [11], WC [12], and SiO_2 film [7]. However, most of them are used for catalyst. Although Novak et al. reported ALD Pt nanoparticles for memory applications, their study relates only to deposition cycles rather than the effect of substrate temperature and pulse time of the precursor on the growth behavior of Pt nanoparticles [7]. Moreover, the ALD technique is also attempted to grow other metallic nanodots for memory applications, such as Ru, WN, and RuO_x nanodots [13-15]. It is worthwhile to mention that by means of the ALD technique, high-density metal nanodots can be obtained at much lower temperatures compared to high-temperature RTA of ultrathin metal films [16,17]. On

* Correspondence: sjding@fudan.edu.cn
State Key Laboratory of ASIC and System, School of Microelectronics, Fudan University, Shanghai 200433, China

low-voltage operation, recent efforts have been focused on high-*k* dielectrics to replace SiO_2 as a gate oxide in nanodot floating gate memories [6]. Among high-*k* dielectrics, Al_2O_3 has been widely studied due to its dielectric constant of approximately 9, a large bandgap of 8.9 eV, a large band offset of 2.8 eV with respect to silicon, good chemical and thermal stabilities with the silicon substrate, and amorphous matrix at high temperature [18]. Therefore, in this article, the ALD growth of Pt nanodots on Al_2O_3 films has been investigated comprehensively, and the experimental parameters are optimized for high-density Pt nanodots. Further, metal-oxide-semiconductor (MOS) capacitors with Pt nanodots have been fabricated, and the corresponding memory characteristics are measured.

Methods

Firstly, around 8-nm Al_2O_3 films were deposited on cleaned P-type silicon substrates by ALD using the precursors Al $(CH_3)_3$ and water. Subsequently, the ALD growth of Pt nanodots were carried out on the surface of Al_2O_3 film using (MeCp)Pt(Me)$_3$ and O_2 precursors in a commercial tool (TFS 200, Beneq, Vantaa, Finland). Herein, the precursor (MeCp)Pt(Me)$_3$ was kept at 70°C, the vapor of which was pulsed into the reaction chamber by the carrier gas argon (99.999%). High-purity O_2 (99.999%) was pulsed into the reaction chamber through a separate gas line with a flow rate of 100 sccm. During the ALD process, the working pressure in the deposition chamber was maintained at 5 mbar, and the O_2 pulse time was fixed at 0.1 s. To obtain the optimal process conditions, the influences of substrate temperature, pulse time of (MeCp)Pt(Me)$_3$, and reaction cycles on Pt nanodot growth were investigated respectively. Further, to investigate the characteristics of Pt nanodots as charge storage nodes, the Al gate MOS capacitors with 8-nm Al_2O_3/Pt nanodots/24-nm Al_2O_3 were fabricated; herein, Pt nanodots were deposited under optimized conditions (shown later). As a comparison, a MOS capacitor without Pt nanodots was also fabricated.

The thicknesses of Al_2O_3 film was measured by an ellipsometer (SOPRA GES 5E, Courbevoie, France). ALD of Pt was characterized by field emission scanning electron microscope (FE-SEM; JSM-6700 F, JEOL, Tokyo, Japan), high-resolution transmission electron microscope (HR-TEM), and X-ray photoelectron spectroscopy (XPS) (Kratos Axis Ultra DLD). Capacitance-voltage (*C-V*) measurements were performed on a LCR meter (Keithley 590, Cleveland, OH, USA), and voltage pulses were generated by a pulse/pattern generator (Keithley Model 3402).

Results and discussion

Impact of substrate temperature on ALD Pt nanodots

Figure 1 shows the Pt 4*d* XPS spectra of the deposited Pt at different substrate temperatures. It is found that

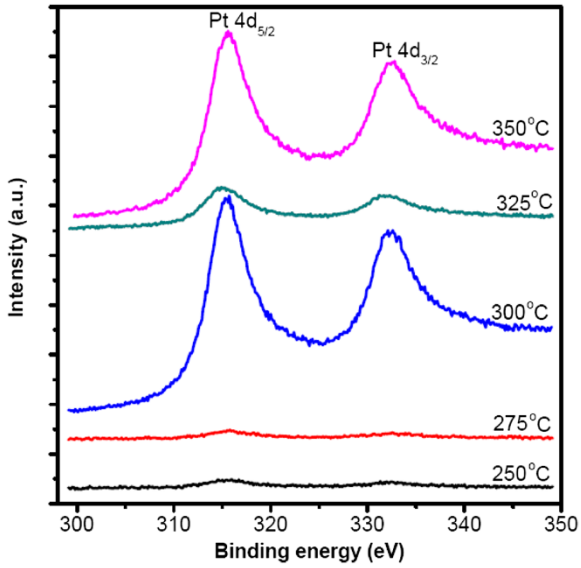

Figure 1 Pt 4*d* XPS spectra of ALD Pt on Al_2O_3 film at different substrate temperatures. Deposition cycles 70.

the peaks of Pt 4*d* are negligible in the case of 250°C and 275°C, indicating the growth of a few Pt atoms. Aaltonen et al. also reported that only very thin Pt films were obtained at 250°C compared to the deposition temperature of 300°C [19]. This could be attributed to the factor that low temperature cannot stimulate effectively the half reaction between (MeCp)Pt(Me)$_3$ and Pt-O_x, which is described as $CH_3C_5H_4Pt(CH_3)_3$ + Pt-O_x → Pt (s) + CO_2 (g) + H_2O (g) + other by-products, where the Pt-O_x species represents oxygen adsorbed on the Pt surface [20]. When the substrate temperature was increased to 300°C, very strong photoelectron peaks associated with Pt $4d_{5/2}$ and $4d_{3/2}$ were observed, indicating the deposition of a mass of Pt atoms. However, the Pt 4*d* peaks decreased again when the substrate temperature was increased to 325°C, revealing a reduced deposition of Pt. As suggested in [19], during the following (MeCp)Pt(Me)$_3$ pulse, the ligands react with the adsorbed oxygen layer. However, it is reported that oxygen can be desorbed from a Pt surface at 330°C [21]; therefore, it is likely that oxygen desorption also occurs at 325°C in our case. This will lead to a limited amount of oxygen on the Pt surface, thus reducing the reaction probability and the deposition of Pt as well. On the other hand, the thermal decomposition of (MeCp)Pt(Me)$_3$ can also take place to some extent at a substrate temperature of 325°C [19]; this results in an additional deposition of Pt. In a word, the behavior of ALD Pt was determined by the aforementioned two competitive processes, and the former is likely dominant in the present experiment. When the substrate temperature goes up to 350°C, the resulting Pt 4*d* peaks become strong again. This should be ascribed to thermal

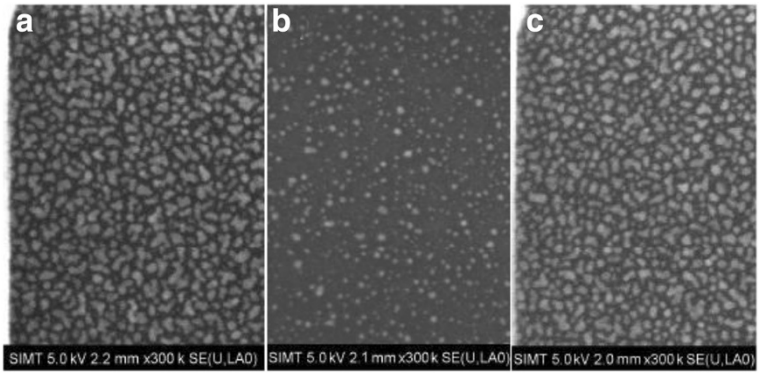

Figure 2 SEM images of ALD Pt on the Al_2O_3 surface corresponding to different substrate temperatures. (**a**) 300°C, (**b**) 325°C, and (**c**) 350°C.

decomposition of (MeCp)Pt$(Me)_3$, thus resulting in the deposition of a mass of Pt atoms, as reported in the literature [19,22,23].

In order to observe intuitively the formation of Pt nanodots, the surface morphologies of the Pt samples deposited at different temperatures were measured by SEM. In terms of substrate temperatures of 250°C and 275°C, the resulting SEM images do not show any nanodots (not shown here). Regarding the substrate temperature of 300°C, lots of Pt nanodots are observed on the surface of Al_2O_3, as shown in Figure 2a. When the substrate temperature increased to 325°C, the density and size of the deposited Pt nanodots became small, see Figure 2b. As the substrate temperature rose to 350°C, the resulting Pt nanodots become denser and bigger again, shown in Figure 2c. The aforementioned phenomena are in good agreement with the XPS spectra in Figure 1. Consequently, to achieve high-density Pt nanodots, the substrate temperature of 300°C is much preferred.

Influence of (MeCp)Pt$(Me)_3$ pulse time on ALD Pt nanodots

With respect to a real ALD process, it is very important to employ enough pulse lengths of precursors to saturate the surface adsorption and ensure the monolayer growth. However, as for the growth of high-density metal nanodots, the density of Pt nuclei on the substrate surface is a key point, which depends on the substrate surface chemistry, the precursor activities, and the pulse length. In general, when the Pt nuclei at the surface are very dense, the resulting Pt might be in the form of a film. Contrarily, if the Pt nuclei are very sparse, the deposited Pt appears in the form of nanodots with a low density, which will not be able to meet the requirement of a memory device. Therefore, to achieve high-density Pt nanodots, the influence of the pulse time of (MeCp)Pt$(Me)_3$ on ALD Pt nanodots should be investigated while maintaining constant O_2 pulse time. Figure 3 shows the survey XPS spectra of the deposited Pt samples corresponding to different pulse times of (MeCp)Pt$(Me)_3$ in the case of 70 deposition cycles. It is seen that the intensity ratio of Pt $4p_{3/2}$ to O 1*s* peaks increases distinctly with an increase of the (MeCp)Pt$(Me)_3$ pulse time from 0.25 s to 1.5 s. This reflects a marked increase of Pt coverage on the surface of the Al_2O_3 film. When the pulse time is further increased to 2 s, the aforementioned intensity ratio exhibits a slight increase. Meanwhile, it is observed that the peaks of Pt 4*d* exhibit remarkable enhancement in comparison with those corresponding to 1.5-s pulse time. This indicates that when the pulse time exceeds 1.5 s, the Pt deposition is dominated by its growth on the surface of Pt nanodots

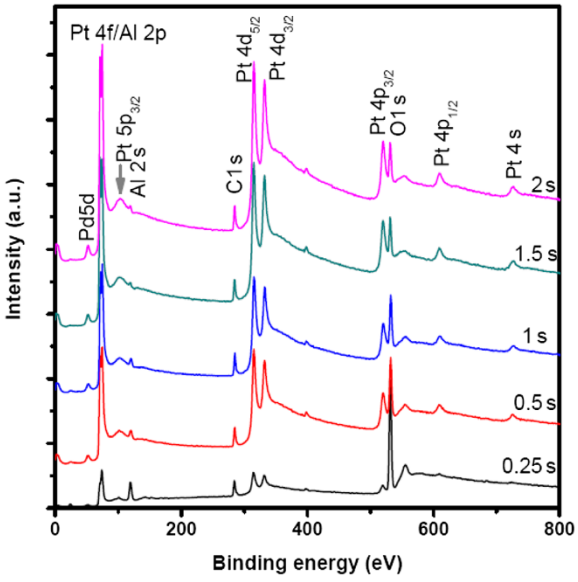

Figure 3 Survey XPS spectra of ALD Pt on Al_2O_3 film as a function of (MeCp)Pt$(Me)_3$ pulse time. Substrate temperature 300°C, deposition cycles 70.

due to the fact that most of the Al_2O_3 surface has been covered by ALD Pt, thus likely leading to the preferential vertical growth of Pt.

Figure 4 shows the surface SEM images of the deposited Pt nanodots corresponding to different pulse times of $(MeCp)Pt(Me)_3$ respectively. In the case of 0.25-s pulse time, the resulting Pt nanodots are very small, sparse, and nonuniform. Nevertheless, when the pulse time increases to 0.5 s, the resulting Pt nanodots become much denser and bigger, thus revealing that the pulse time of $(MeCp)Pt(Me)_3$ plays a key role in the growth of Pt nanodots. Further, as the pulse time increases gradually to 2 s, the resulting Pt nanodots do not exhibit distinct changes based on the SEM images, but it is believed that the distances between nanodots become narrower and narrower, and even the coalescence between adjacent nanodots could occur. Therefore, to ensure the growth of high-density Pt nanodots, the coalescence between adjacent nanodots should be avoided during ALD. For this purpose, the pulse time of $(MeCp)Pt(Me)_3$ should be controlled between 0.5 and 1 s.

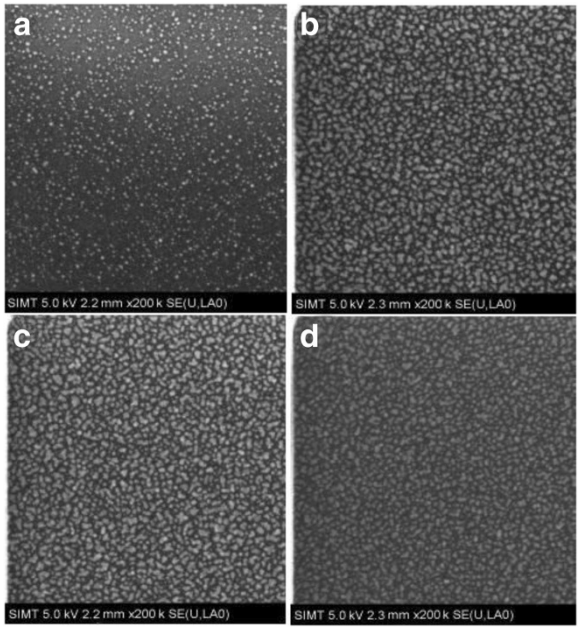

Figure 4 SEM images of ALD Pt on Al_2O_3 for different pulse times of $(MeCp)Pt(Me)_3$. (**a**) 0.25, (**b**) 0.5, (**c**) 1, and (**d**) 2 s (substrate temperature 300°C, deposition cycles 70).

Influence of deposition cycles on ALD Pt

Figure 5 illustrates the surface morphologies of the resulting Pt nanodots as a function of deposition cycles. In the case of ≤60 deposition cycles, the deposited Pt nanodots exhibit low densities and small dimensions. When the number of deposition cycles increases to 70, the density of Pt nanodots increases remarkably. As the deposition duration reaches 90 cycles, the resulting Pt nanodots exhibit much larger dimensions and irregular shapes as well as a reduced density.

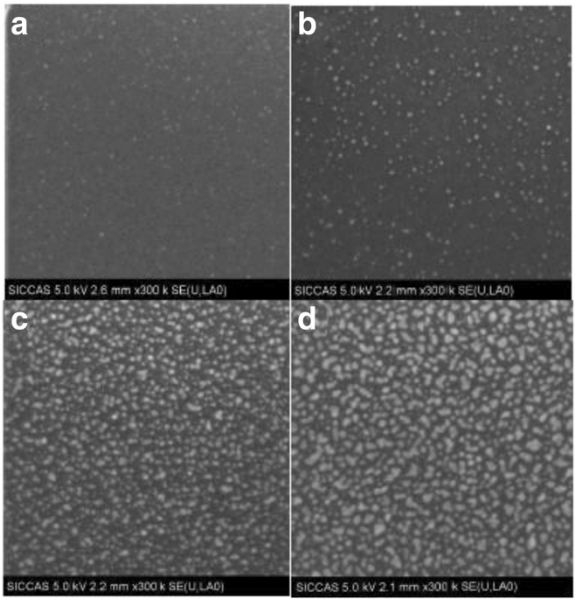

Figure 5 SEM images of ALD Pt on Al_2O_3 as a function of deposition cycles. (**a**) 40, (**b**) 60, (**c**) 70, and (**d**) 90 cycles. Substrate temperature, 300°C; pulse time of $(MeCp)Pt(Me)_3$, 1 s.

Further, the planar TEM images of the Pt nanodots corresponding to 70 and 90 cycles are compared in Figure 6. It is found that the Pt nanodots corresponding to 70 deposition cycles exhibit a density as high as approximately 2×10^{12} cm^{-2} and a well-separated distribution, and most of them appear in the form of a sphere. In addition, an electron diffraction image of the selected area shows that the Pt nanodots are polycrystalline. However, for 90 deposition cycles, the resulting Pt nanoparticles exhibit various irregular shapes such as sphere, ellipse, bar, etc. The observed decrease in the density of Pt nanoparticles should be attributed to the coalescence between adjacent nanodots, which is incurred by a long deposition time. Based on the above discussion, 70 deposition cycles are advisable to achieve high-density Pt nanodots on the surface of Al_2O_3. On the other hand, it should be noticed that the substrate surface has a great influence on the growth of metal nanodots. As an example, compared to the surface of ALD Al_2O_3 film, the surfaces of thermal SiO_2 and H-Si -terminated silicon are not in favor of the growth of Pt and Ru nanodots and thus cannot achieve high-density nanodots [7,16]. This is due to the fact that the surface chemistry determines the initial nucleation of metal.

As the deposition cycles increase continuously, the Pt particles become bigger and bigger, and the probability

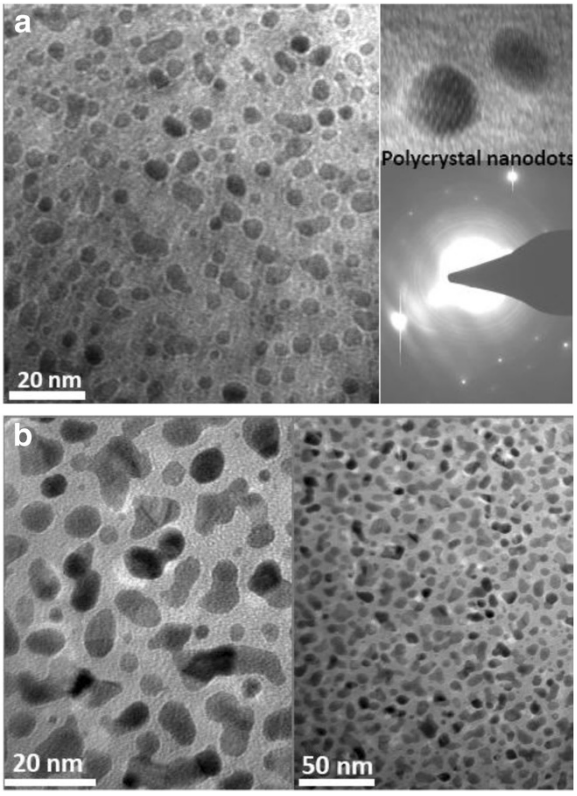

Figure 6 Planar TEM images of ALD Pt on Al_2O_3 film. Corresponding to (**a**) 70 cycles, together with an electron diffraction image of selected area, and (**b**) 90 cycles.

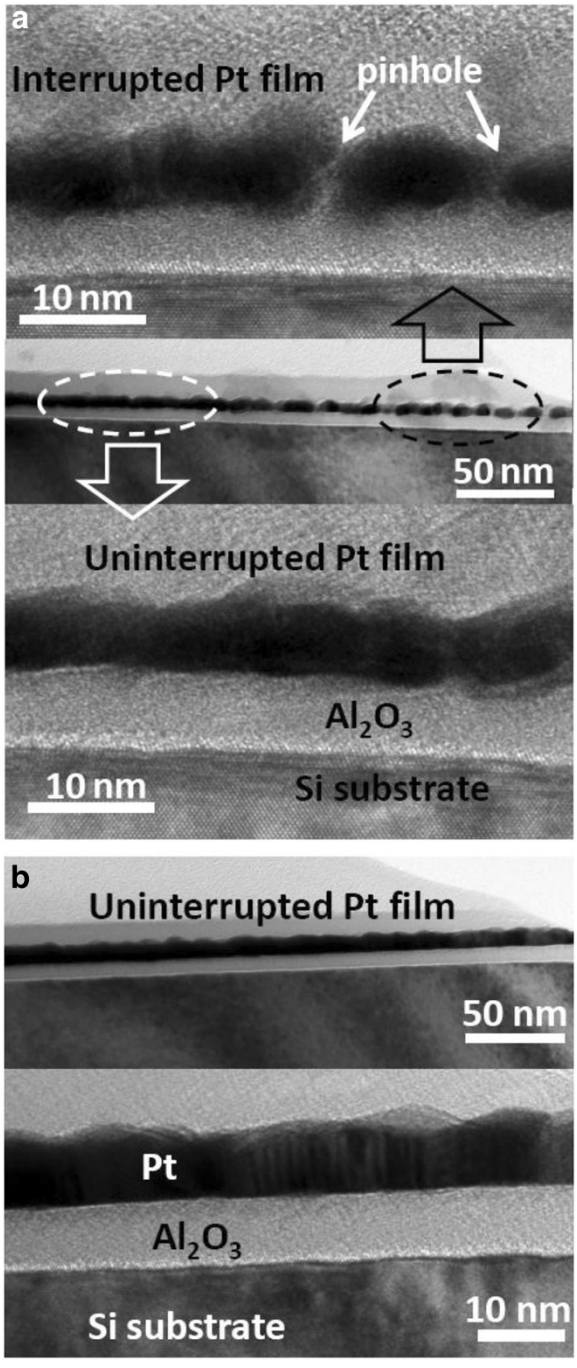

Figure 7 Cross-sectional TEM images of ALD Pt corresponding to different deposition cycles. (**a**) 120 and (**b**) 200 cycles.

of coalescence between Pt particles increases gradually. As shown in Figure 7a, when the deposition cycles increase up to 120, a discontinuous Pt thin film is formed, i.e., the Pt film is interrupted by pinholes in some regions. Further, a perfect Pt film without any pinholes is formed when the deposition duration reaches 200 cycles, shown in Figure 7b.

Memory characteristics of MOS capacitors with Pt nanodots

Figure 8 shows the *C-V* hysteresis curves of the MOS capacitor with Pt nanodots in comparison with the counterpart without Pt nanodots. It is indicated that the capacitor with Pt nanodots exhibits a hysteresis window as much as 10.2 V in the case of +15 V to −15 V of scanning voltage. However, the hysteresis window for the capacitor without Pt nanodots is as small as 0.28 V. This reveals that the Pt nanodots have significant charge trapping capability.

In order to investigate the programmable and erasable characteristics of the memory capacitor, the MOS capacitor with Pt nanodots was programmed and erased, respectively, under different voltages for 1 ms, as shown in Figure 9. It is found that the resulting *C-V* curve shifts noticeably towards a positive bias with increasing the programming voltage from +8 to +12 V, see Figure 9a. This indicates that the probability of electrons injected from the substrate is enhanced with increasing the gate voltage, which is due to a reduction of the Fowler-Nordheim tunneling barrier through the tunneling Al_2O_3 layer. On the contrary, as the erasing voltage

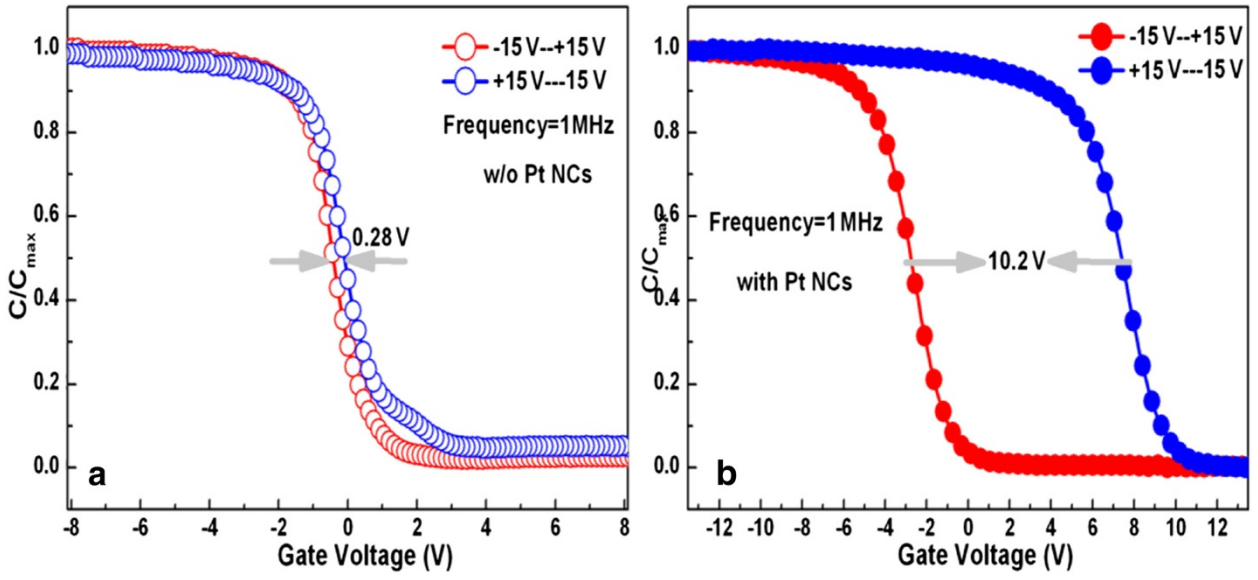

Figure 8 High-frequency (1 MHz) *C-V* hysteresis curves of the MOS capacitors. (**a**) Without Pt nanodots and (**b**) with Pt nanodots.

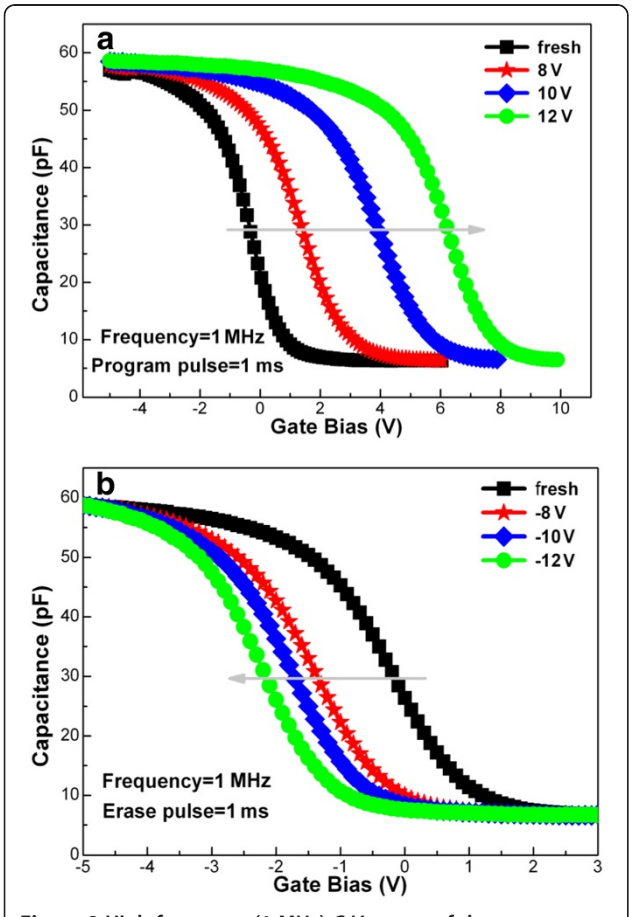

Figure 9 High-frequency (1 MHz) *C-V* curves of the memory capacitor. Corresponding to (**a**) programming and (**b**) erasing under different gate voltage for 1 ms, respectively.

changes from −8 to −12 V, the resulting *C-V* curve moves gradually in the direction of negative bias, see Figure 9b. This reveals hole trapping and electron de-trapping in the MOS structure. In a word, our experimental results indicate that the MOS capacitor with Pt nanodots can be programmed and erased efficiently even under low voltages of ±8 V, and the resulting memory window is as large as 2.8 V for 1 ms of programming/erasing time.

Figure 10 shows the charge retention characteristics of the MOS capacitor with Pt nanodots at room temperature. It is seen that the memory window is close to 8.2 V after programming/erasing under ±12 V for 1 ms, and the deduced memory window still approaches 5.6 V after 10 years by extrapolation. This indicates

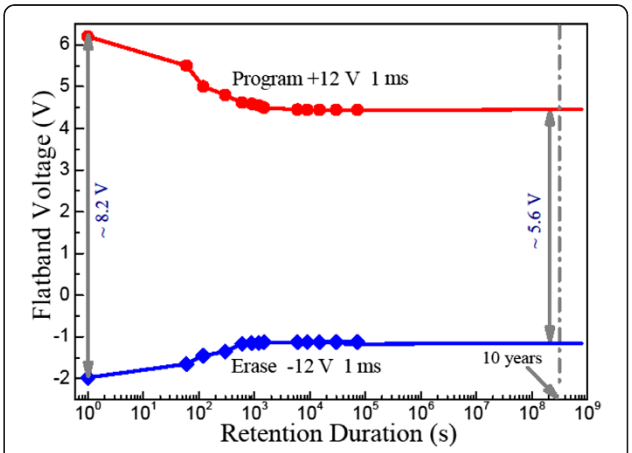

Figure 10 Charge retention characteristics of the MOS capacitor with Pt nanodots at room temperature.

that Pt nanodots can offer not only enough capability for electron storage but also good charge retention characteristic.

Conclusions

Growth of Pt nanodots on the surface of Al_2O_3 has been investigated by ALD using $(MeCp)Pt(Me)_3$ and O_2 precursors. By optimizing substrate temperature, pulse time of $(MeCp)Pt(Me)_3$, and deposition cycles, Pt nanodots with a high density of approximately 2×10^{12} cm^{-2} have been achieved, i.e., the process parameters are as follows: substrate temperature 300°C, $(MeCp)Pt(Me)_3$ pulse time 1 s, and 70 deposition cycles. Further, the fabricated MOS capacitor with Pt nanodots exhibits noticeable programmable and erasable characteristics even under low voltages of ±8 V, a large memory window, and good charge retention at room temperature.

Competing interests

The authors declare that they have no competing interests.

Authors' contributions

SJD carried out the main part of the experimental design and analytical works and drafted the manuscript. HBC carried out the fabrication and electrical measurements and some of the analytical works. XMC, SC, QQS, PZ, HLL, DWZ, and CS gave their good comments and suggestions during this study. All authors read and approved the final manuscript.

Acknowledgments

The authors thank the financial support of the National Key Technologies R&D Program (2009ZX02302-002), National Natural Science Foundation of China (no. 61076076, 61274088), the Program for New Century Excellent Talents in University (NCET-08-0127), and the Key Project of the Chinese Ministry of Education (108052).

Received: 30 November 2012 Accepted: 8 January 2013
Published: 15 February 2013

References

1. Gu DF, Baumgart H, Tapily K, Shrestha P, Namkoon1 G, Ao XY, Müller F: **Precise control of highly ordered arrays of nested semiconductor/metal nanotubes.** *Nano Res* 2011, **4:**164–170.
2. Jiang XR, Huang H, Prinz FB, Bent SF: **Application of atomic layer deposition of platinum to solid oxide fuel cells.** *Chem Mater* 2008, **20:**3897–3905.
3. Liu C, Wang CC, Kei CC, Hsueh YC, Perng TP: **Atomic layer deposition of platinum nanoparticles on carbon nanotubes for application in proton-exchange membrane fuel cells.** *Small* 2009, **5:**1535–1538.
4. Yang DQ, Zhang GX, Sacher E: **Evidence of the interaction of evaporated Pt nanoparticles with variously treated surfaces of highly oriented pyrolytic graphite.** *J Phys Chem B* 2006, **110:**8348–8356.
5. Singh PK, Bisht G, Auluck K, Sivatheja M, Hofmann R, Singh KK, Mahapatra S: **Performance and reliability study of single-layer and dual-layer platinum nanocrystal flash memory devices under NAND operation.** *IEEE Trans Electron Devices* 2010, **57:**1829–1837.
6. Kim H, Woo S, Kim H, Bang S, Kim Y, Choi D, Jeon H: **Pt nanocrystals embedded in remote plasma atomic-layer-deposition HfO_2 for nonvolatile memory devices.** *Electrochem Solid-State Letters* 2009, **12:**H92.
7. Novak S, Lee B, Yang X, Misra V: **Platinum nanoparticles grown by atomic layer deposition for charge storage memory applications.** *J Electrochem Soc* 2010, **157:**H589–H592.
8. Yeom D, Kang J, Lee M, Jang J, Yun J, Jeong DY, Yoon C, Koo J, Kim S: **ZnO nanowire-based nano-floating gate memory with Pt nanocrystals embedded in Al_2O_3 gate oxides.** *Nanotechnology* 2008, **19:**395204.
9. Lee C, Meteer J, Narayanan V, Kan EC: **Self-assembly of metal nanocrystals on ultrathin oxide for nonvolatile memory applications.** *J Electron Mater* 2005, **34:**1–11.
10. Li J, Liang XH, King DM, Jiang YB, Weimer AW: **Highly dispersed Pt nanoparticle catalyst prepared by atomic layer deposition.** *Appl Catal Environ* 2010, **97:**22–226.
11. Christensen ST, Elam JW, Rabuffetti FA, Ma Q, Weigand SJ, Lee B, Seifert S, Stair PC, Poeppelmeier KR, Hersam MC, Bedzyk MJ: **Controlled growth of platinum nanoparticles on strontium titanate nanocubes by atomic layer deposition.** *Small* 2009, **5:**750–757.
12. Hsu IJ, Hansgen DA, McCandless BE, Willis BG, Chen JG: **Atomic layer deposition of Pt on tungsten monocarbide (WC) for the oxygen reduction reaction.** *J Phys Chem C* 2011, **115:**3709–3715.
13. Farmer DB, Gordon RG: **High density Ru nanocrystal deposition for nonvolatile memory applications.** *J Appl Phys* 2007, **101:**124503.
14. Lim SH, Joo KH, Park JH, Lee SW, Sohn WH, Lee C, Choi GH, Yeo IS, Chung UI, Moon JT, Ryu BI: **Nonvolatile MOSFET memory based on high density WN nanocrystal layer fabricated by novel PNL (pulsed nucleation layer) method.** In *Symposium on VLSI Technol. Digest of Technical Papers: June 14–16 2005*. New York: IEEE; 2005:190–191.
15. Maikap S, Wang TY, Tzeng PJ, Lin CH, Lee LS, Yang JR, Tsai MJ: **Charge storage characteristics of atomic layer deposited RuO_x nanocrystals.** *Appl Phys Lett* 2007, **90:**253108.
16. Zhang M, Chen W, Ding SJ, Wang XP, Zhang W, Wang LK: **Investigation of atomic-layer-deposited ruthenium nanocrystal growth on SiO_2 and Al_2O_3 films.** *J Vac Sci Technol A* 2007, **25**(4):775–780.
17. Gou HY, Ding SJ, Huang Y, Sun QQ, Zhang W, Wang PF, Chen Z: **Nonvolatile metal–oxide–semiconductor capacitors with Ru-RuO_x composite nanodots embedded in atomic-layer-deposited Al_2O_3 films.** *J Electron Mater* 2010, **39**(8):1343–1350.
18. Gou HY, Chen S, Ding SJ, Sun QQ, Lu HL, Zhang W, Wang PF: **Influence of HfAlO composition on memory effects of metal-oxide-semiconductor capacitors with Al_2O_3/HfAlO/Al_2O_3 layers and Pd electrode.** *Thin Solid Films* 2012, doi: 10.1016/j.tsf.2012.07.071.
19. Aaltonen T, Ritala M, Sajavaara T, Keinonen J, Leskelä M: **Atomic layer deposition of platinum thins films.** *Chem Mater* 2003, **15:**1924–1928.
20. Hiratani M, Nabatame T, Matsui Y, Imagawa K, Kimura S: **Platinum film growth by chemical vapor deposition based on autocatalytic oxidative decomposition.** *J Electrochem Soc* 2001, **148**(8):C524–C527.
21. Ohno Y, Matsushima T: **Dissociation of oxygen admolecules on platinum (110)(1 X-2) reconstructed surfaces at low-temperatures.** *Surf Sci* 1991, **241**(1–2):47–53.
22. Knoops HCM, Mackus AJM, Donders ME, Sanden MCM, Notten PHL, Kessels WMM: **Remote plasma ALD of platinum and platinum oxide films.** *Electrochem Solid-State Lett* 2009, **12:**G34–G36.
23. Jiang X, Bent SF: **Area-selective atomic layer deposition of platinum on YSZ substrates using microcontact printed SAMs.** *J Electrochem Soc* 2007, **154:**D648.

doi:10.1186/1556-276X-8-80
Cite this article as: Ding *et al.*: Atomic layer deposition of high-density Pt nanodots on Al_2O_3 film using $(MeCp)Pt(Me)_3$ and O_2 precursors for nonvolatile memory applications. *Nanoscale Research Letters* 2013 **8**:80.